

Article

# Uptake of Pb(II) Ions from Simulated Aqueous Solution via Nanochitosan

Camellia Zareie <sup>1</sup>, Saeideh Kholghi Eshkalak <sup>2,3</sup>, Ghasem Najafpour Darzi <sup>4,\*</sup>, Mazyar Sharifzadeh Baei <sup>5</sup>, Habibollah Younesi <sup>6</sup>  and Seeram Ramakrishna <sup>3,\*</sup>

<sup>1</sup> Department of Chemical Engineering, Faculty of Chemical Engineering, Tarbiat Modares University, Tehran 14115-114, Iran; zareie.chpre@gmail.com

<sup>2</sup> Department of Polymer Engineering and Color Technology, Amirkabir University of Technology, 424 Hafez Ave, Tehran 15875-4413, Iran; s.kholghi143@gmail.com

<sup>3</sup> Department of Mechanical Engineering, Center for Nanofibers and Nanotechnology, Faculty of Engineering, National University of Singapore, Singapore 117576, Singapore

<sup>4</sup> Faculty of Chemical Engineering, Babol Noshirvani University of Technology, Shariati Avenue, Babol 47148-71167, Iran

<sup>5</sup> Chemical Engineering Department, Ayatollah Amoli Branch, Islamic Azad University, Amol 14778-93855, Iran; mazyar.sharifzadeh@gmail.com

<sup>6</sup> Department of Environmental Science, Faculty of Natural Resources, Tarbiat Modares University, Noor 46414-356, Iran; hunesi@modares.ac.ir

\* Correspondence: najafpour@nit.ac.ir (G.N.D.); seeram@nus.edu.sg (S.R.)

Received: 10 November 2019; Accepted: 12 December 2019; Published: 15 December 2019



**Abstract:** In this work, nanochitosan (NC) was prepared through ionic gelation using low molecular weight chitosan and maleic acid (MA). The synthesized NC was characterized by atomic force microscopy (AFM), Fourier transform infrared spectroscopy (FTIR), and scanning electron microscopy (SEM). During preparation, the particle size of the material depended on parameters such as concentration of chitosan and pH of the aqueous solution. After controlling the mentioned parameters, NC smaller than 100 nm was prepared. The chitosan and prepared NC were employed for the adsorption of Pb(II) from an aqueous solution in the form of a batch system. Among the sorption parameters, pH showed the strongest effect on the sorption process and removal of the maximum number of Pb(II) ions was obtained at pH value of 6. Pseudo-first-order and pseudo-second-order models were used to track the kinetics of the adsorption process. Langmuir and Freundlich's isotherms were subjected to the absorption data to evaluate absorption capacity. NC proved to be an excellent adsorbent with a remarkable capacity to eliminate Pb(II) ions from aqueous solutions at multiple concentrations. The NC also showed better performance with a comparatively easier preparation process than in other reported work.

**Keywords:** adsorption; chitosan; isotherm; nanochitosan; Pb(II) ion removal

## 1. Introduction

Contamination from heavy metals is considered a serious threat to the environment and public health because of their non-biodegradability, high toxicity, and organism bioaccumulation [1]. Generally, heavy metals are very toxic and can cause serious damage to living organisms even at low concentrations [2]. Pb(II), a heavy metal, can cause irreversible damage to the brain as well as the nervous and kidney systems following entry into the human body. These damages may cause cancer, amnesia, and mental retardation [3]. Due to Pb(II)'s high toxicity, the United States Environmental Protection Agency (USEPA) has set a very low tolerance limit of Pb(II) (0.015 mg/L) for drinking water [4]. Various techniques are used for the removal of heavy metals from water and wastewater,

including chemical sedimentation [5], ion exchange [6], membrane [7], and adsorption [8–11]. Among them, adsorption is appealing owing to its simple application, low cost, and remarkable efficiency. These characteristics have made it a center of attention for the synthesis and preparation of novel and efficient adsorbents in recent decades [2]. Various types of adsorbents such as carbon active [6], nanotube [9], and bentonite [10] have been widely used for the treatment of water and wastewater, especially for the removal of Pb(II) ion.

Chitosan constructs with randomly distributed beta D-glucosamine (deacetylated unit) and N-acetyl-D-glucosamine known as a linear polysaccharide. It is commonly produced by the reaction of the chitin (made from shrimp and other crustacean shells) with a chemical alkaline-based substance (commonly sodium hydroxide) [12]. Because of the free protonate amine groups in its structure, chitin is soluble in acidic solutions and insoluble in aqueous solutions [13]. The recent widespread application of chitosan for the metal ion elimination from the aqueous phase is due to the existence of hydroxyl and amine groups in its chemical structure, having a high potential to bind with metal ions [4,14]. Chitosan's excessive sensitivity to pH makes it adopt the form of a gel or become dissolved at various pH values [15]. In order to overcome this challenge, crosslinked chitosan is used instead of conventional untreated chitosan [4,16], such as glyoxal, formaldehyde, glutaraldehyde, and isocyanate [17–19]. Some crosslinked chitosans have been used as adsorbents for the removal and purification of water and wastewater from metal ions. For instance, Kyzas et al. synthesized two new cross-linked chitosans and used them for the adsorption of Cd<sup>2+</sup> and Pb<sup>2+</sup> ions [20]; this resulted in a considerably improved adsorption capacity after crosslinking. A crosslinked magnetic chitosan has also been prepared and applied for adsorption of an aqueous solution containing Pb<sup>2+</sup> [2]. The synthesized nanochitosan (NC) with its smaller size indicates high stability in the wide range of pH. Due to this high stability, nanochitosan can be described as a good candidate for various purposes including water and wastewater treatment [21]. The nanochitosan has been widely used in various fields, including tissue engineering, enzyme immobilization support, cancer diagnosis, and antioxidant activity [22].

Due to effect of pH on chitosan's structure, crosslinked chitosans are widely synthesized and used. The synthesis of crosslinked chitosan is not simple and requires special agents. The size of the crosslinked chitosan (<100 nm) is also an important parameter for its application, especially in the medical and biomedical fields. In this study, a one-step simple process was used for the preparation of nanochitosan by the addition of K<sub>2</sub>S<sub>2</sub>O<sub>8</sub> as the crosslinking agent into a chitosan solution. The primary aim was to produce NC smaller than 100 nm to be used in various fields. To evaluate the effect of experimental conditions on nanoparticles' size and aggregation, the samples were characterized with advanced techniques such as Fourier transform infrared spectroscopy (FTIR), scanning electron microscopy (SEM), and atomic force microscopy (AFM). The second purpose of this study was to pick up Pb<sup>2+</sup> ions from an aqueous solution by NC in a batch process. The effect of pH, dosage of NC, and exposure time to metal ion absorption were investigated. In addition, adsorption isotherms and kinetics were studied.

## 2. Experimental Section

### 2.1. Materials

Chitosan (molecular weight (MW) = 50–190 kDa), with a degree of acetylation (75–85%) was purchased from Sigma-Aldrich (St. Louis, MO, USA). Maleic acid (MA) and lead nitrate were purchased from Merck (Darmstadt, Germany).

### 2.2. Preparation of NC

NC was synthesized pursuant to a developed procedure by de Moura et al. [23–26]. Initially, chitosan and MA were dissolved in distilled water and then stirred for 30 min in a stirrer (VELP Scientifica, Usmate, Italy) at 300 rpm. Subsequently, K<sub>2</sub>S<sub>2</sub>O<sub>8</sub> (0.2 mmol) was mixed into the mixture under vigorous stirring at 70 °C for 7 h; this was followed by cooling the mixture in a cool

bath until a milky emulsion was obtained. The suspension was centrifuged for 15 min at 16,000 rpm and then placed in a freeze dryer [24]. Figures 1 and 2 present the maleic acid polymerization mechanism and chitosan-MA nanoparticle formation.

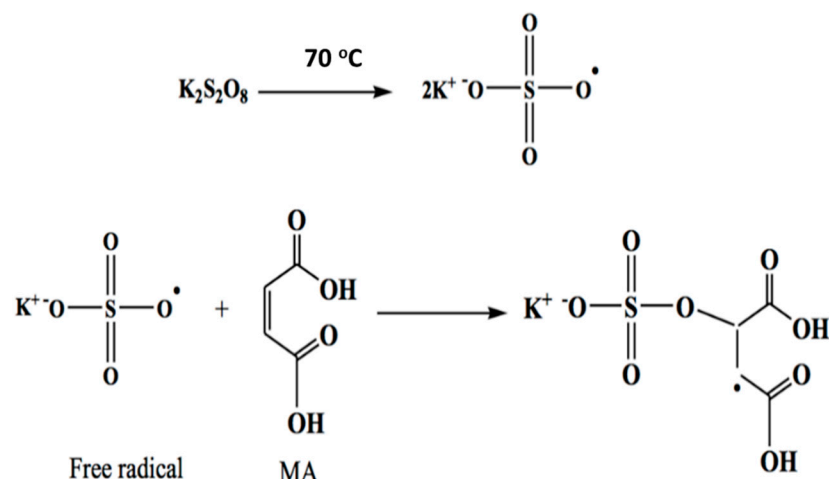


**Figure 1.** Schematic of maleic acid polymerization mechanism.

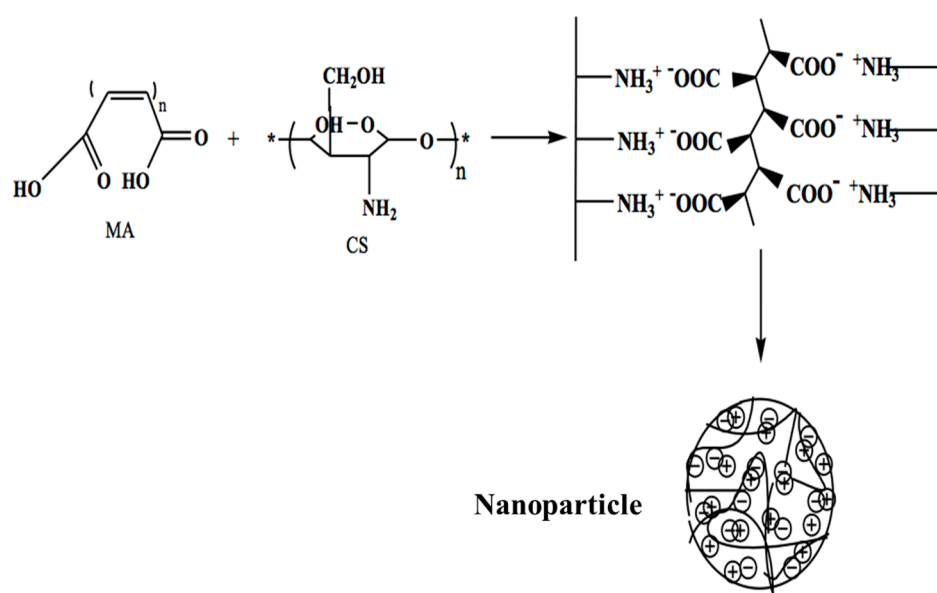


**Figure 2.** Schematic of chitosan-MA nanoparticle formation.

### 2.3. Characterizations of Chitosan and NC

The morphologies of the chitosan surface and NC samples were analyzed using scanning electron microscopy (SEM) with a KYKY model EM3200 microscope (KYKY, Beijing, China). For the SEM analysis, the sample was placed in a vacuum and operated at a 25 kV acceleration voltage. FTIR analyses of chitosan and NC were done by a Shimadzu Spectrum model 8400s (Kyoto, Japan) in the spectra range of 4000 to 400  $\text{cm}^{-1}$ . The concentration of Pb(II) was determined by a SensAA atomic absorption spectrometer (GBC Scientific Equipment, Sydney, Australia), equipped with a lead hollow cathode lamp in the aqueous media.

### 2.4. Batch Experiment

All experiments of the adsorption kinetics of Pb(II) ions on chitosan and NC adsorbent were carried out in a batch reactor at room temperature. The adjustment of solution pH was done by adding

1 M HCl and 1 M NaOH solutions. In all of the above experiments, the amount of metal ions adsorbed was calculated according to Equation (1) as follows:

$$q_e = (C_0 - C_e) \times \frac{V}{m} \quad (1)$$

where  $q_e$  (mg/g),  $C_0$  and  $C_e$  (mg/L),  $V$  (L) and  $m$  (g) are the adsorption capacity, initial and final metal concentrations in the aqueous solution, volume of the solution, and mass of the adsorbent, respectively. The removal efficiency ( $R$ ) was calculated as follows:

$$R = \frac{C_0 - C_f}{C_0} \times 100\% \quad (2)$$

$C_f$  is final concentration.

### 3. Results and Discussion

#### 3.1. Synthesis of Nanochitosan

Fan et al. [25] found that the synthesis of nanochitosan depended on the concentration of chitosan in the solution, mass ratio of chitosan to crosslinking agent, and pH of the solution. Hence, to prevent microparticle formation, synthesis parameters such as the concentration of chitosan, the concentration of crosslinking agent, and the adjustment of pH in solution should be done. The morphology of the prepared NC samples in various ranges of chitosan concentrations and pH of the solution was evaluated by SEM. In this study, the pH adjustment was in the range of 3 to 6 and the mass ratio of chitosan/MA was 2:1 and 1:1. In the acid solution, the amine groups in chitosan and carboxyl groups in MA were protonated with a possible influence on the size of the nanoparticles. Figures 1 and 2 show a typical schematic of chitosan-MA nanoparticle formation. They demonstrate the formation of MA-chitosan nanoparticles via the polymerization of MA in the presence of chitosan molecules for electrostatic interactions. At a certain level of MA polymerization, the formation of chitosan-MA nanoparticles occurs with linkages between negatively charged MA carboxyl groups and chitosan amine groups.

As seen in Figure 3, the shape and structure of NC are affected remarkably by the chitosan/MA mass ratio. At the chitosan/MA mass ratio of 1:1, the ratio of  $\text{NH}_2/\text{COOH}$  is 0.5. As can be seen, due to the higher ratio of the MA acid functional group compared to the chitosan functional group at this mass ratio, the polymerization of MA (instead of NC production) occurs and, subsequently, an extensive aggregation of products is observed. The NCs are produced by the binding between the carboxyl in MA and the protonated amine in the chitosan group. When the ratio of the functional group of chitosan is higher than or equal to MA, the whole amount of MA contributes in the reaction with the amine functional group of chitosan. The main purpose of this research was to synthesize the NC from chitosan and test its application for the removal of Pb(II) from an aqueous solution. Therefore, for the production of NC, a mass ratio of 2:1 was selected for chitosan/MA. As shown in Figures 3 and 4, the nanoparticle size increases by increasing pH from 3 to 6. There are two reasons for this behavior. First, increasing the pH of the solution may also lead to an increase in degrees of ionization and charge density of the MA molecules. Hence, the repulsive electrostatic forces of the internal MA molecules rise, causing an inflation in the nanoparticles and an increase in particle size. Second, the reduction in chitosan's solubility by increasing the pH may increase the adhesion and aggregation of nanoparticles. The results indicate that the increase in particle size is due to increased chitosan concentration.

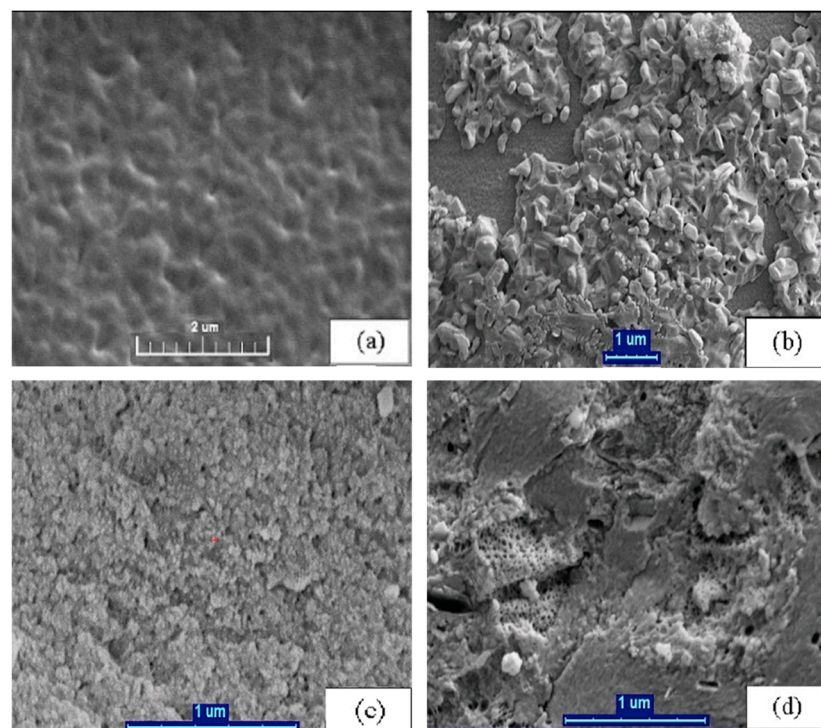


**Figure 3.** Scanning electron microscopy (SEM) of nanochitosan in mass ratio of chitosan/MA = 1 and at several pH values of (a) 3, (b) 4, (c) 5, and (d) 6.

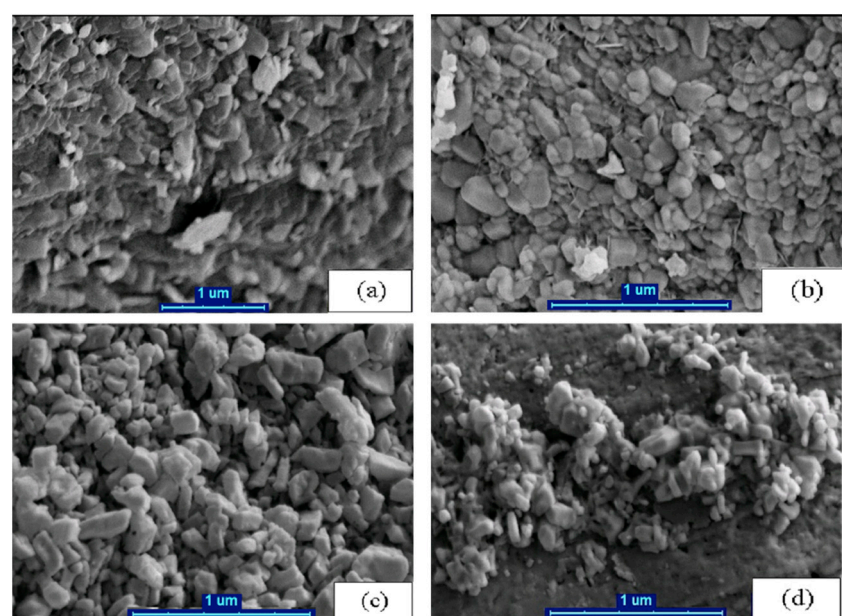


**Figure 4.** SEM of nanochitosan (NC) in mass ratio of chitosan/MA = 2 and at several pH values of (a) 3, (b) 4, (c) 5, and (d) 6.

The SEM image of chitosan is shown in Figure 5. Chitosan presents a nonporous and smooth morphology, whereas the SEM image of NC exhibits a porous and chain-like morphology.

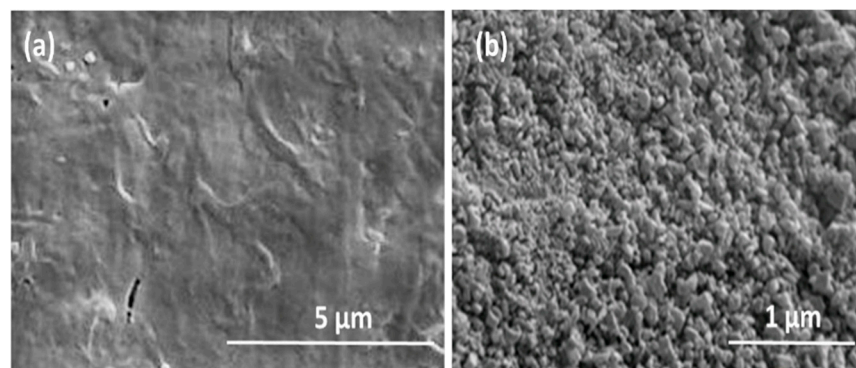


**Figure 5.** SEM of (a) chitosan and (b) NC (mass ratio of chitosan/MA = 2:1, pH = 4).

It was found that increasing the pH caused the NC's diameter to increase, to more than 180 nm (Figures 6 and 7). The best result was obtained at pH = 4 and a mass ratio of chitosan/MA = 2.

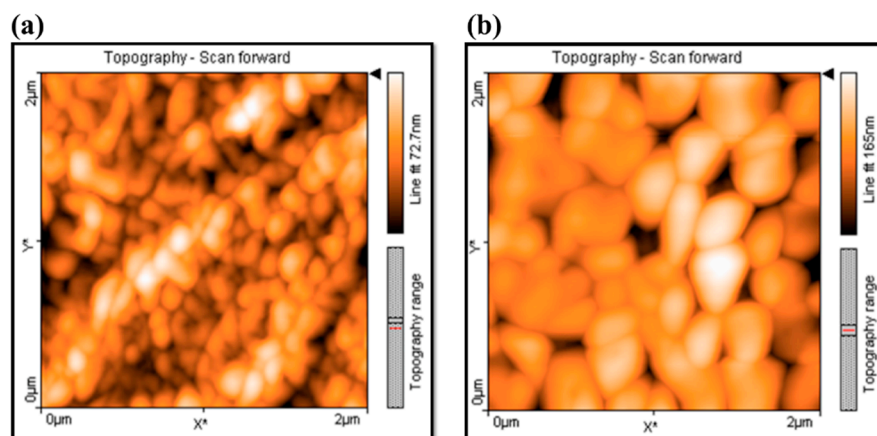


**Figure 6.** Atomic force microscopy (AFM) images of NC in mass ratio of chitosan/MA = 2:1 and (a) pH = 4, (b) pH = 5.

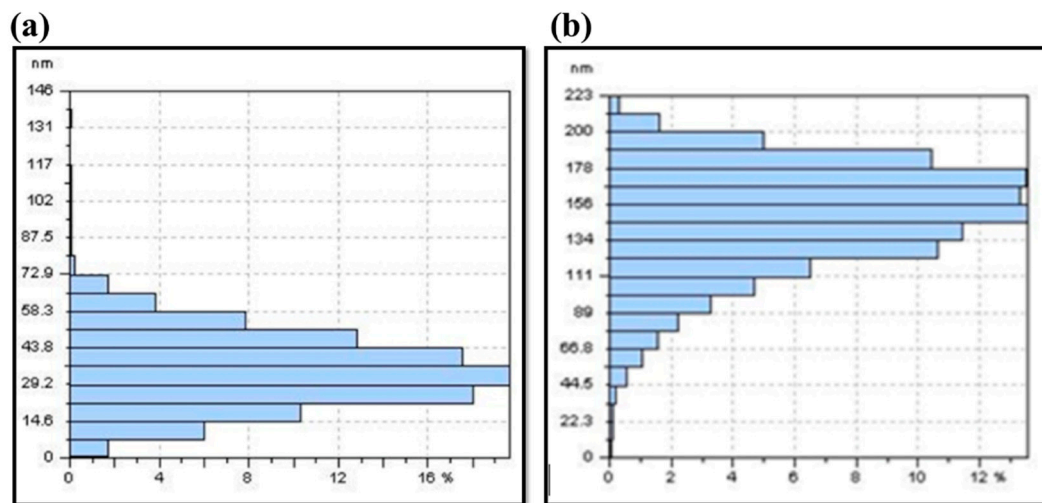


**Figure 7.** Nanochitosan size distribution in mass ratio of chitosan/MA = 2:1 and (a) pH = 4, (b) pH = 5.

At the end of the production process, colloidal suspension opalescence was observed, as a confirmation of the end of the process. Figure 8 clearly shows good stability of the nanoparticles in suspension after 22 days, confirming the suspension's applicability in different fields, namely pharmacy (a solution is required instead of solid particles). It is interesting to observe that the nanoparticles

were formed spontaneously without the need for high temperature treatment or application of organic solvents.

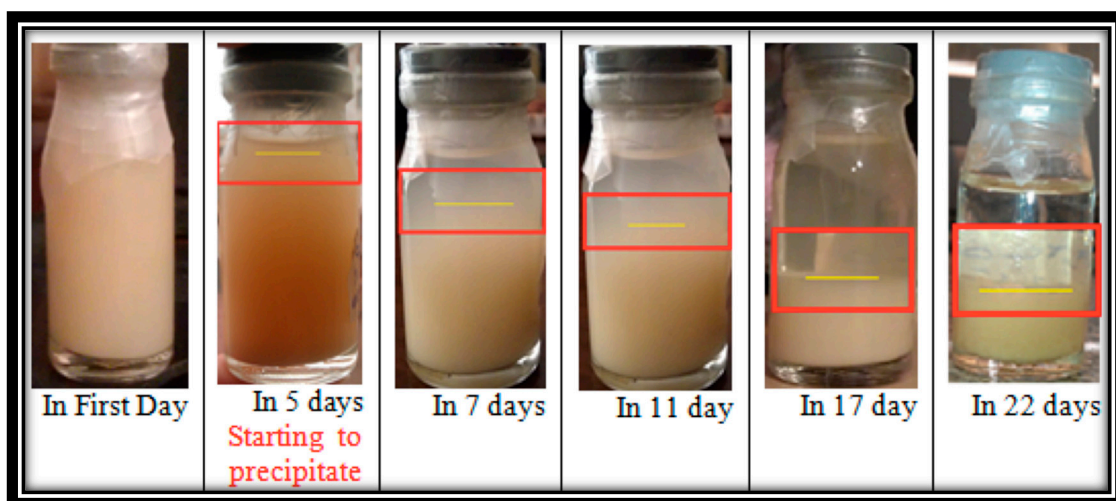


**Figure 8.** Stability of chitosan-MA nanoparticle solution (mass ratio 1:1, pH = 4).

Figure 9 displays an FTIR spectrum of NC with various functional groups. The chitosan spectrum presents a characteristic peak at  $3435\text{ cm}^{-1}$  corresponding to the stretching vibration of  $\text{NH}_2$  and OH groups, whereas the bands at  $1660$  and  $3050\text{ cm}^{-1}$  correspond to N–H and the  $\text{NH}_2$  groups; the one at  $1700\text{ cm}^{-1}$  is related to C=O and that at  $1080\text{ cm}^{-1}$  corresponds to the stretching vibration of C–O. The appearance of two new bands was observed at  $1638$  and  $1545\text{ cm}^{-1}$  due to groups of  $\text{COO}^-$  and  $\text{NH}^{3+}$ , respectively. These clearly demonstrated the ionic interaction between MA and particles of chitosan to form the NC particles [26]. The presence of MA in the nanoparticles' compositions is proven by the bands at  $1700$  and  $1600\text{ cm}^{-1}$ , corresponding to C=O and C–C.

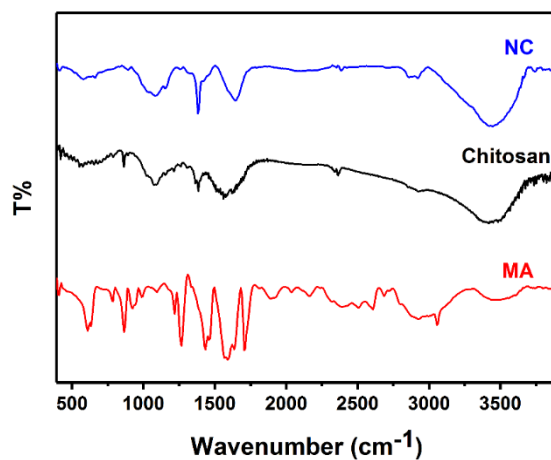


**Figure 9.** Fourier transform infrared spectroscopy (FTIR) spectra of maleic acid, chitosan, and NC.

### 3.2. Effect of Chitosan and NC in Adsorption of Pb(II) Ions from Aqueous Solution

#### 3.2.1. Effect of pH

One of the important parameters in the processing of adsorption is the pH of the aqueous media, which directly affects the chemical structure of metal ions and active sites of adsorbents [27]. Figure 10 shows the effect of various pH values on the adsorption of Pb(II) ions through NC and chitosan. By increasing the pH to 6, the efficiency of removal increased dramatically. Above pH = 6.0, Pb(II) ions precipitated in the hydroxide form [28,29]. At pH of 6, the efficiency levels of Pb(II) ion removal for

NC and chitosan were 93.88% and 66.32%, respectively. At pH less than 4, the adsorption rate was very low since the adsorbent's surface was completely covered with  $\text{H}^+$ , which competed strongly with  $\text{Pb}(\text{II})$  ions for sites of adsorption, hence the possibility of  $\text{Pb}(\text{II})$  adsorption was minimized [30]. In the  $4 < \text{pH} < 6$  range, the  $\text{H}^+$  ion concentration decreased and  $\text{Pb}(\text{II})$  ions were more likely to be adsorbed on active sites of NCs or Cs. Hence, for the adsorption of  $\text{Pb}(\text{II})$  ions, the optimum pH was defined at 6; thus, this pH was selected for all other experiments in this work.

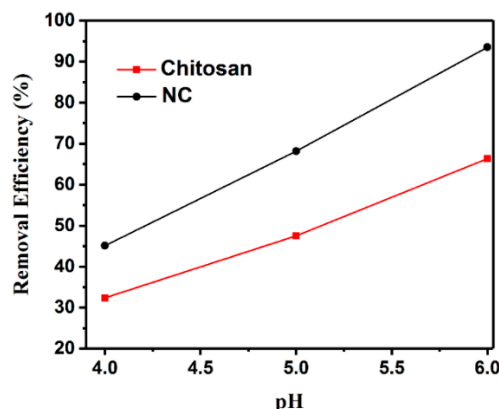


**Figure 10.** Effect of various pH values on the removal efficiency of  $\text{Pb}(\text{II})$  ions by NC and chitosan (in the initial concentration, 10 mg/L; adsorbent mass, 2.5 g/L; rate of shaking, 180 rpm; and temperature, 298 K).

### 3.2.2. Effect of Contact Time

Figure 11 shows the role of chitosan and NC on the removal efficiency of metal ions. The results indicated that the adsorption process underwent two stages. The first or initial rapid adsorption stage accounted for a large part of the total adsorption. The removal rate was high and the majority of metal ions were adsorbed in the first 30 min. The second stage had a smaller share of adsorption in which the processing of adsorption was slow, and equilibrium was observed in less than 1 and 1.5 h for NC and chitosan, respectively. Therefore, for further experiments, the selected contact times were 60 and 90 min for NC and chitosan, respectively. However, it has been reported that a long time was required for metal sorption from aqueous solutions by chitosan [31]; in contrast, in the present investigation, the removal of lead ions from aqueous solutions was obtained in a short contact time. This was attributed to the large surface area and high surface reactivity of NC. The results also illustrated that the lead ion adsorption capacity of NC was superior to that of chitosan.

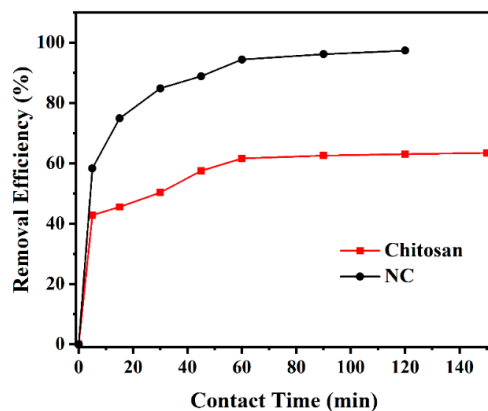


**Figure 11.** Effect of contact time on the removal efficiency of  $\text{Pb}(\text{II})$  ions by NC and chitosan (in the initial concentration, 10 mg/L; adsorbent mass, 2.5 g/L; rate of shaking, 180 rpm; and temperature, 298 K).

### 3.2.3. Kinetics of Adsorption

The kinetics of adsorption provides significant data about the reaction paths and the rate of the process. To determine the controlling mechanism for the processing of adsorption, both pseudo-first-order (Equation (3)) and pseudo-second-order (Equation (4)) kinetic models were applied [32,33]:

$$\log(q_e - q_t) = \log q_e - \frac{k_1}{2.303} t \quad (3)$$

$$\frac{t}{q_t} = \frac{1}{k_2 q_e^2} + \frac{t}{q_e} \quad (4)$$

where  $q_t$  (mg/g),  $q_e$  (mg/g),  $k_1$  ( $\text{min}^{-1}$ ),  $k_2$  ( $\text{g}\cdot\text{mg}^{-1}\cdot\text{min}^{-1}$ ), and  $t$  (min) show the amount of metal ion adsorbed, adsorption capacity at adsorption equilibrium, kinetic rate constants for the pseudo-first-order and the pseudo-second-order models, and time of contact, respectively.

In the present investigation, the adsorption data were used to examine the amount of lead ions adsorbed before a contact time, for initial concentrations of metal ions in the range of 10 to 100 mg/L. The uptake of lead ions increased with the contact time and the system reached equilibrium after 60 min for NC and 90 min for chitosan. Increasing metal ion concentration in the aqueous solution increased the chance of an effective collision between the metal ions and the adsorbent and resulted in improved metal ion removal.

Table 1 presents the calculated data for kinetic adsorption of Pb(II) ions that were fitted to Equations (3) and (4). A comparison between the observed and the calculated values of  $q_t$  against time revealed a very good fit with the pseudo-second-order rate equation compared with the pseudo-first-order rate equation for both adsorbents. Therefore, the adsorption of lead ions is well illustrated by the pseudo-second-order kinetic model (Figures 12 and 13). The constants of pseudo-second-order rate are slightly different for the five initial lead ion concentrations, which reflects the inferior effect of initial concentration. Adoption of the pseudo-second-order kinetic model means that the rate-limiting step may be chemisorption involving valence forces through the sharing or exchanging of electrons between adsorbent and adsorbate [34]. It was found that the adsorption data fitted well with pseudo-first-order and pseudo-second-order kinetics at high and low initial pollutant concentrations, respectively [35,36].

**Table 1.** Kinetic parameters of the adsorption of Pb(II) ions using chitosan and NCs.

Sorbent	Initial Pb(II) Conc. (mg/L)	$q_e, \text{exp}$ (mg/g)	Pseudo-First-Order Model			Pseudo-Second-Order Model		
			$k_1$ ( $\text{min}^{-1}$ )	$q_{e1}$ (mg/g)	$R^2$	$k_2$ ( $\text{g}\cdot\text{mg}^{-1}\cdot\text{min}^{-1}$ )	$q_{e2}$ (mg/g)	$R^2$
Chitosan	10	2.50	0.0576	1.894	0.908	0.0905	2.60	0.997
	30	6.83	0.0484	5.483	0.932	0.0207	7.30	0.994
	50	10.15	0.0253	6.792	0.930	0.0992	10.87	0.994
	75	11.88	0.0258	9.528	0.957	0.0521	13.16	0.986
	100	12.60	0.0207	13.122	0.938	0.0226	15.87	0.975
NCs	10	3.62	0.0759	2.761	0.949	0.0833	3.77	0.998
	30	10.26	0.0806	8.414	0.984	0.0322	10.64	0.998
	50	16.45	0.0956	15.78	0.969	0.0192	17.24	0.998
	75	22.12	0.0553	19.498	0.984	0.0752	23.26	0.997
	100	25.82	0.0598	21.281	0.971	0.0525	27.78	0.996

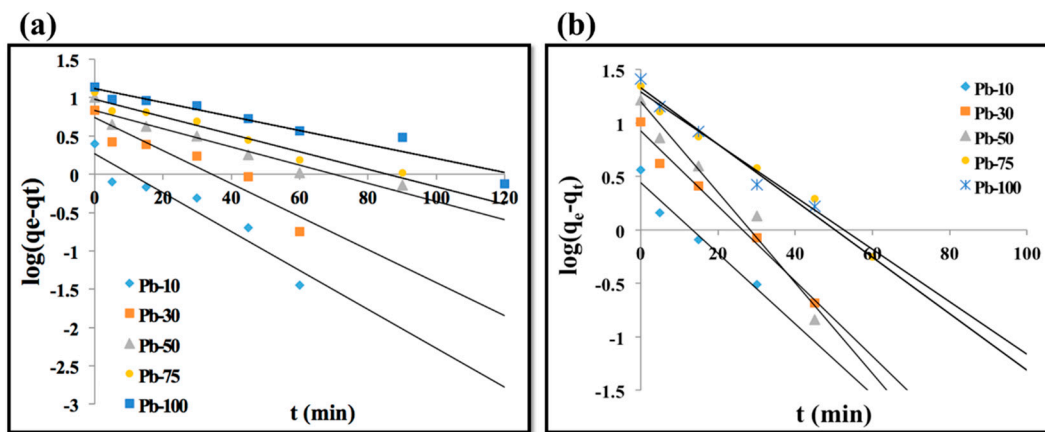


**Figure 12.** Pseudo-first-order model of (a) chitosan and (b) NC for Pb(II) ions ( $\text{pH} = 6$ ; adsorbent mass, 2.5 g/L; rate shaking, 180 rpm; temperature, 298 K).

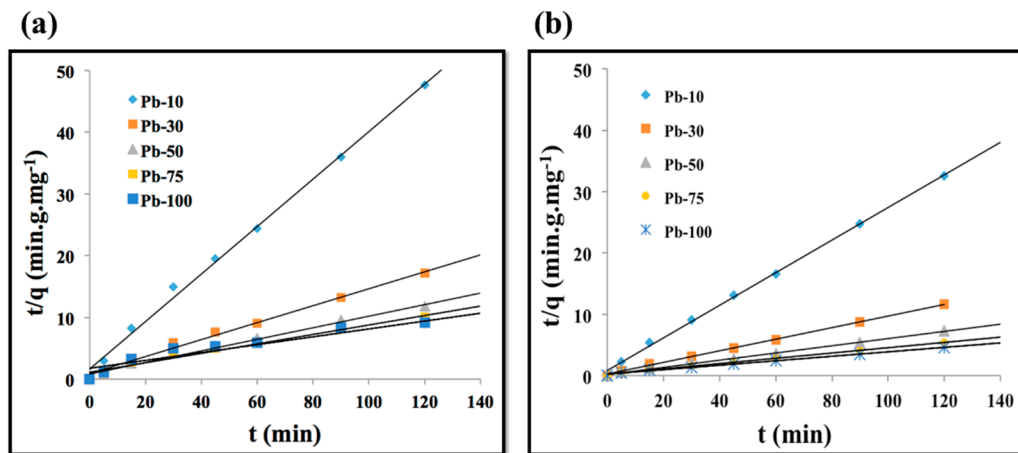


**Figure 13.** Pseudo-second-order model of (a) chitosan and (b) NC for Pb(II) ions ( $\text{pH} = 6$ ; adsorbent mass, 2.5 g/L; rate of shaking, 180 rpm; temperature, 298 K).

### 3.2.4. Adsorption Isotherms

The adsorption isotherm model is essential in order to predict and compare the performance of adsorbents. Equilibrium studies have described the affinity and surface properties of adsorbents by constant values and characterized the adsorption capacity of adsorbents [37–41]. Langmuir and Freundlich models as adsorption isotherms were studied at concentrations of different initial lead ions in the range of 10–100 mg/L on NC and chitosan (Figures 14 and 15). The expressions of the Langmuir isotherm and the linear form of this isotherm are presented in Equations (5) and (6):

$$q_e = \frac{q_m K_L C_e}{1 + K_L C_e} \quad (5)$$

$$\frac{C_e}{q_e} = \frac{1}{K_L q_m} + \frac{C_e}{q_m} \quad (6)$$

where  $q_e$  is the adsorption capacity (mg/g) and  $C_e$  is the equilibrium adsorbent concentration (mg/L), while the maximum adsorption capacity of adsorbents (mg/g) is shown by  $q_m$ . The affinity of binding sites is represented by  $K_L$  as the Langmuir constant (L/mg) and is a scale of adsorption energy. The Langmuir isotherm model assumes that the maximum adsorption capacity happens on a monolayer of the adsorbent surface. This model states that all adsorption sites have equal energy and that intermolecular forces decrease with increasing distance from the adsorption surface.

The Freundlich isotherm model presumes that adsorption happens at multilayers and various adsorbent sites have different energies. Equations (7) and (8) show the Freundlich isotherm model and its linear form:

$$q_e = K_F C_e^{\frac{1}{n}} \quad (7)$$

$$\ln q_e = \ln K_F + \frac{1}{n} \ln C_e \quad (8)$$

where the  $n$  and  $K_F$  (mg/g) are Freundlich constants related to the adsorption intensity and adsorption capacity, respectively. Figure 14a,b presents Langmuir and Freundlich linear fittings, respectively, whereas the isotherm constants are presented in Table 2. Based on the regression factor ( $R^2$ ), it was observed that the Langmuir model's experimental data were better than those of the Freundlich model for both NC and chitosan, implying the predominant occurrence of the monolayer adsorption. The fact that the Langmuir isotherm fitted well to the experimental data may also be due to the homogenous distribution of active sites on NC and chitosan (the Langmuir equation obtains a homogenous surface) [39]. The maximum adsorption capacity ( $q_m$ ) obtained from the Langmuir isotherm was 32.26 mg/g. The magnitude of the exponent  $n$  shows the favorability of adsorption;  $n > 1$  and  $n < 1$  represent good and poor adsorption characteristics, respectively. Freundlich and Langmuir adsorption isotherms generally indicate the surface heterogeneity and homogeneity, respectively [42,43].

**Table 2.** Parameters of the isotherm models for  $\text{Pb}^{2+}$  adsorption.

Adsorbent	Langmuir Isotherm		Freundlich Isotherm			
	$q_m$ (mg/g)	$K_L$ (L/mg)	$R^2$	$n$	$K_F$ (mg/g)	$R^2$
NCs	32.26	0.1188	0.997	1.790	4.140	0.975
Chitosan	16.39	0.055	0.991	1.78	1.422	0.905

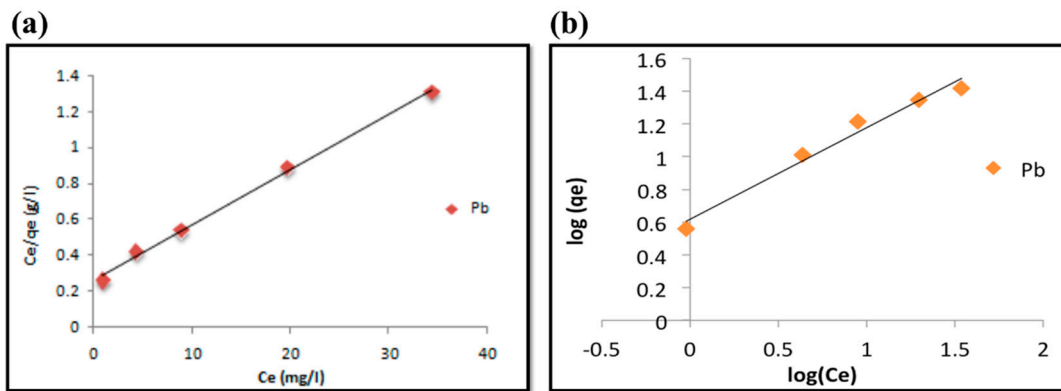


**Figure 14.** (a) Langmuir isotherm plot and (b) Freundlich isotherm plot for the adsorption of  $\text{Pb}(\text{II})$  ions on NC.

The Brunauer-Emmett-Teller (BET) model was used to determine the monolayer capacity per unit bulk mass of the adsorbed molecules. The BET model follows from Equation (9):

$$\frac{C_e}{q_e(C_s - C_e)} = \frac{1}{q_s C_{BET}} + \frac{(C_{BET} - 1)}{q_s C_{BET}} \frac{C_e}{C_s} \quad (9)$$

where  $C_e$  is the equilibrium concentration (mg/L),  $C_s$  is the adsorbate monolayer saturation concentration (mg/L), and  $C_{BET}$  is the BET adsorption isotherm related to the surface interaction energy (L/mg). The  $q_e$  is adsorption capacity in equilibrium condition.

One of the modified Langmuir equations is the Toth isotherm, which caused a reduction of error in the experimental and predicted data. This model is the most appropriate method in adsorbate

concentration and explains that a system of heterogeneous adsorption satisfies both low and high boundaries. The Toth isotherm model is stated below:

$$\frac{q_e}{q_m} = \theta = \frac{K_e C_e}{[1 + (K_L C_e)^n]^{1/n}} \quad (10)$$

where  $K_e$ ,  $K_L$  and  $n$  are Toth isotherm constants ( $\text{mg}\cdot\text{g}^{-1}$ ). The parameter  $n$  is a heterogeneity characteristic; when  $n = 1$ , this equation converts to the Langmuir isotherm equation and, on the other hand, the system is heterogeneous if it deviates further away from unity (1). In this model, the parameters can be examined by a nonlinear curve-fitting method with a sigma plot software (version 14). In addition, for several adsorption multilayer systems, a heterogeneous isotherm of the Toth model has been applied.

Notwithstanding the accessibility of many isotherm models, the Dubinin-Astakhov (DA) model is the most suitable candidate for volume filling of micropores and the adsorption into mesopores and macropores. Moreover, the DA model accounts for the energetic surface heterogeneity of the adsorbents. Furthermore, in order to allow a basic increase in the activation energy in the finest micropores, the DA model uses the Weibull distribution to describe the degree of adsorption with regard to the energy of adsorption. The DA model was introduced in the following form:

$$n = n_0 \exp\left\{-B\left(\ln\left(\frac{C_o}{C_e}\right)\right)^k\right\} \quad (11)$$

where  $n_0$  is the maximum capacity per unit aggregate mass of the adsorbed probe molecules at the end of adsorption and  $B$  and  $k$  are fitting parameters. The  $C_o$  is initial concentration.

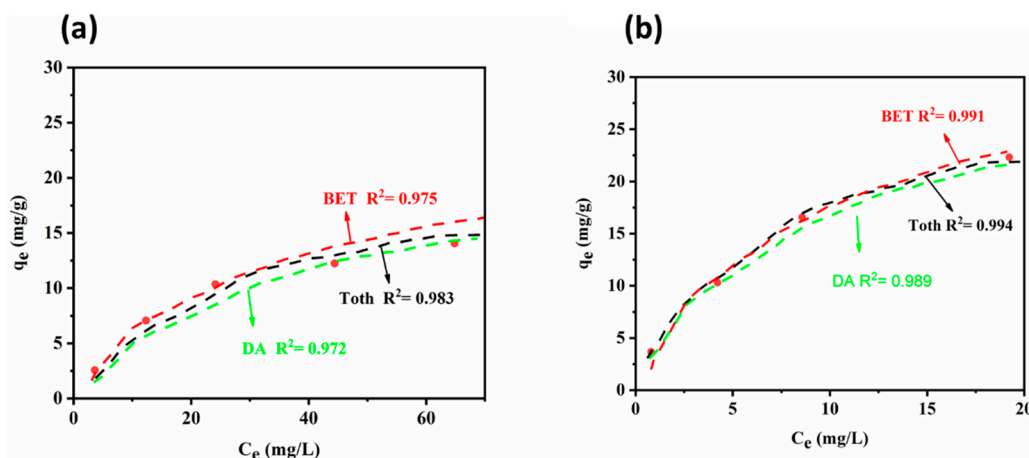


**Figure 15.** The isotherm plots of (a) NC and (b) chitosan for the adsorption of Pb(II) ions.

Figure 15 shows the data fitting for these isotherms. As can be seen, the equilibrium data fitted well with these isotherms. However, the Toth model showed a better fitting in comparison with the BET and DA models.

### 3.3. Comparison between NC Adsorption Capacity and Other Adsorbents

In order to better understand NC's adsorption capacity, the obtained experimental results were compared with several adsorbents, such as chitosan–pectin pellets, chitosan crosslinked with chitosan crosslinked with Epichlorohydrin (ECH), Procion Green H-4G immobilized poly(2-hydroxyethyl methacrylate) (pHEMA)/chitosan, crosslinked carboxymethyl-chitosan resin, pristine chitosan, and copolymer 2-hydroxyethyl methacrylate with monomer methyl methacrylate. Table 3 shows the experimental results of several adsorbents based on the adsorption capacity. As can be seen from Table 3, the adsorption capacity of the synthesized NC in this study was much better than adsorbents such as

chitosan-pectin pellets, crosslinked carboxymethyl-chitosan resin, and pristine chitosan. However, NC showed inferior adsorption capacity to chitosan crosslinked with ECH and Procion Green H-4G immobilized pHEMA/chitosan. It should be mentioned that NC, in this study, was synthesized by a simple and easy process, whereas the synthesis procedures of chitosan crosslinked with ECH or Procion Green H-4G immobilized pHEMA/chitosan are not simple.

**Table 3.** Comparison between NC and other adsorbents.

Adsorbent	Pb(II) $q_e$	Ref.
Chitosan	13.1 mg/g	[37]
Chitosan-pectin pellets	11.9 mg/g	[38]
Chitosan crosslinked with ECH	34.13 mg/g	[37]
Procion Green H-4G immobilized pHEMA + chitosan	68.81 mg/g	[39]
Crosslinked carboxymethyl-chitosan resin	0.15 mmol/g	[40]
Copolymer 2-hydroxyethyl methacrylate with monomer methyl methacrylate	31.5 mg/g	[41]
NC	32.26 mg/g	This study

As shown in Table 3, modified chitosan such as nanochitosan adsorbent has a greater capacity to adsorb metal ions from the aqueous solution in comparison to other types of synthesized chitosan. It should be mentioned that the synthesis of NC in this study was performed by a one-step simple process that can be easily used for the synthesis process on a large scale.

#### 4. Conclusions

Chitosan nanoparticles were successfully obtained from the polymerization of MA in a solution consisting of CS. The particle size is highly dependent on the chitosan concentration used in the preparation method and is greatly influenced by the pH of the solution. From SEM and AFM analyses, it can be concluded that morphology and particle size distribution of nanochitosan are very homogeneous and uniform. The investigation regarding the capacity of NC application for the removal of Pb(II) ions from an aqueous solution strongly recommended that NCs could be introduced as a suitable adsorbent for the removal of Pb(II) from the aqueous solution. The maximum Pb(II) ion adsorption capacity of NC was very close to other reported chitosans, and superior to some of them. The conditions for the optimal adsorption by NC were as follows: contact time of 60 min and pH of 6 for Pb(II). The experimental results in this work were in good agreement with the theoretical results of the Langmuir isotherm. The kinetic results showed that the adsorption mechanism follows a pseudo-second-order model.

**Author Contributions:** Synthesis and experimental design, C.Z. and G.N.D.; Sample characterization, S.R. and S.K.E.; Writing—original draft, C.Z., S.K.E. and M.S.B.; Writing—review and editing, G.N.D., H.Y. and S.R.

**Funding:** This research received no external funding.

**Acknowledgments:** The authors would like to thank Babol Noshirvani University of Technology, Biotechnology and Nano biotechnology research lab for the facilities provided to conduct the present research.

**Conflicts of Interest:** The authors declare no conflict of interest.

#### References

- Shahzad, A.; Miran, W.; Rasool, K.; Nawaz, M.; Jang, J.; Lim, S.-R.; Lee, D.S. Heavy metals removal by EDTA-functionalized chitosan graphene oxide nanocomposites. *RSC Adv.* **2017**, *7*, 9764–9771. [[CrossRef](#)]
- Shahraki, S.; Delarami, H.S. Magnetic chitosan-(d-glucosamine methyl) benzaldehyde Schiff base for Pb<sup>2+</sup> ion removal. Experimental and theoretical methods. *Carbohydr. Polym.* **2018**, *200*, 211–220. [[CrossRef](#)] [[PubMed](#)]
- Lu, Z.; Tan, R.; Chu, W.; Tang, S.; Xu, W.; Song, W. Synthesis of SrHPO<sub>4</sub>/Fe<sub>3</sub>O<sub>4</sub> magnetic nanocomposite and its application on Pb<sup>2+</sup> removal from aqueous solutions. *Microchem. J.* **2018**, *142*, 152–158. [[CrossRef](#)]

4. Yu, Z.; Dang, Q.; Liu, C.; Cha, D.; Zhang, H.; Zhu, W.; Zhang, Q.; Fan, B. Preparation and characterization of poly(maleic acid)-grafted cross-linked chitosan microspheres for Cd(II) adsorption. *Carbohydr. Polym.* **2017**, *172*, 28–39. [[CrossRef](#)]
5. Rojas, R. Copper, lead and cadmium removal by Ca Al layered double hydroxides. *Appl. Clay Sci.* **2014**, *87*, 254–259. [[CrossRef](#)]
6. Dąbrowski, A.; Hubicki, Z.; Podkościelny, P.; Robens, E. Selective removal of the heavy metal ions from waters and industrial wastewaters by ion-exchange method. *Chemosphere* **2004**, *56*, 91–106. [[CrossRef](#)]
7. Khulbe, K.; Matsuura, T. Removal of heavy metals and pollutants by membrane adsorption techniques. *Appl. Water Sci.* **2018**, *8*, 19. [[CrossRef](#)]
8. Vilela, P.B.; Dalalibera, A.; Duminelli, E.C.; Becegato, V.A.; Paulino, A.T. Adsorption and removal of chromium(VI) contained in aqueous solutions using a chitosan-based hydrogel. *Environ. Sci. Pollut. Res.* **2018**, *26*, 28481–28489. [[CrossRef](#)]
9. Lin, Y.; Ma, J.; Liu, W.; Li, Z.; He, K. Correction to: Efficient removal of dyes from dyeing wastewater by powder activated charcoal/titanate nanotube nanocomposites: Adsorption and photoregeneration. *Environ. Sci. Pollut. Int.* **2019**, *26*, 10274–10275. [[CrossRef](#)]
10. Zou, C.; Jiang, W.; Liang, J.; Sun, X.; Guan, Y. Removal of Pb(II) from aqueous solutions by adsorption on magnetic bentonite. *Environ. Sci. Pollut. Res.* **2019**, *26*, 1315–1322. [[CrossRef](#)]
11. Liu, Y.; Luan, J.; Zhang, C.; Ke, X.; Zhang, H. The adsorption behavior of multiple contaminants like heavy metal ions and p-nitrophenol on organic-modified montmorillonite. *Environ. Sci. Pollut. Res.* **2019**, *26*, 10387–10397. [[CrossRef](#)] [[PubMed](#)]
12. Rinaudo, M. Chitin and chitosan: Properties and applications. *Prog. Polym. Sci.* **2006**, *31*, 603–632. [[CrossRef](#)]
13. Gutha, Y.; Munagapati, V.S. Removal of Pb(II) ions by using magnetic chitosan-4-((pyridin-2-ylimino) methyl) benzaldehyde Schiff's base. *Int. J. Biol. Macromol.* **2016**, *93*, 408–417. [[CrossRef](#)] [[PubMed](#)]
14. Liu, B.; Chen, X.; Zheng, H.; Wang, Y.; Sun, Y.; Zhao, C.; Zhang, S. Rapid and efficient removal of heavy metal and cationic dye by carboxylate-rich magnetic chitosan flocculants: Role of ionic groups. *Carbohydr. Polym.* **2018**, *181*, 327–336. [[CrossRef](#)] [[PubMed](#)]
15. Chiou, M.-S.; Ho, P.-Y.; Li, H.-Y. Adsorption of anionic dyes in acid solutions using chemically cross-linked chitosan beads. *Dye. Pigment.* **2004**, *60*, 69–84. [[CrossRef](#)]
16. Sutirman, Z.A.; Sanagi, M.M.; Karim, J.A.; Naim, A.A.; Ibrahim, W.A.W. New crosslinked-chitosan graft poly(N-vinyl-2-pyrrolidone) for the removal of Cu(II) ions from aqueous solutions. *Int. J. Biol. Macromol.* **2018**, *107*, 891–897. [[CrossRef](#)] [[PubMed](#)]
17. Doshi, B.; Ayati, A.; Tanhaei, B.; Repo, E.; Sillanpää, M. Partially carboxymethylated and partially cross-linked surface of chitosan versus the adsorptive removal of dyes and divalent metal ions. *Carbohydr. Polym.* **2018**, *197*, 586–597. [[CrossRef](#)]
18. Lu, F.; Astruc, D. Nanomaterials for removal of toxic elements from water. *Coord. Chem. Rev.* **2018**, *356*, 147–164. [[CrossRef](#)]
19. Ngah, W.W.; Teong, L.; Hanafiah, M.A.K.M. Adsorption of dyes and heavy metal ions by chitosan composites: A review. *Carbohydr. Polym.* **2011**, *83*, 1446–1456. [[CrossRef](#)]
20. Kyzas, G.Z.; Siafaka, P.I.; Lambropoulou, D.A.; Lazaridis, N.K.; Bikaris, D.N. Poly(itaconic acid)-grafted chitosan adsorbents with different cross-linking for Pb(II) and Cd(II) uptake. *Langmuir* **2014**, *30*, 120–131. [[CrossRef](#)]
21. Hosseini, S.M.; Younesi, H.; Bahramifar, N.; Mehraban, Z. A novel facile synthesis of the amine-functionalized magnetic core coated carboxylated nanochitosan shells as an amphoteric nanobiosupport. *Carbohydr. Polym.* **2019**, *221*, 174–185. [[CrossRef](#)]
22. Divya, K.; Jisha, M.S. Chitosan nanoparticles preparation and applications. *Environ. Chem. Lett.* **2018**, *16*, 101–112. [[CrossRef](#)]
23. Zolfaghari, G.; Esmaili-Sari, A.; Anbia, M.; Younesi, H.; Amirmahmoodi, S.; Ghafari-Nazari, A. Taguchi optimization approach for Pb(II) and Hg(II) removal from aqueous solutions using modified mesoporous carbon. *J. Hazard. Mater.* **2011**, *192*, 1046–1055. [[CrossRef](#)] [[PubMed](#)]
24. Zareie, C.; Najafpour, G. Preparation of nanochitosan as an effective sorbent for the removal of copper ions from aqueous solutions. *Int. J. Eng. Trans. B Appl.* **2013**, *26*, 829–836. [[CrossRef](#)]
25. Fan, W.; Yan, W.; Xu, Z.; Ni, H. Formation mechanism of monodisperse, low molecular weight chitosan nanoparticles by ionic gelation technique. *Colloids Surf. B Biointerfaces* **2012**, *90*, 21–27. [[CrossRef](#)] [[PubMed](#)]

26. de Moura, M.R.; Aouada, F.A.; Mattoso, L.H. Preparation of chitosan nanoparticles using methacrylic acid. *J. Colloid Interface Sci.* **2008**, *321*, 477–483. [[CrossRef](#)]
27. Amini, M.; Younesi, H.; Bahramifar, N.; Lorestani, A.A.Z.; Ghorbani, F.; Daneshi, A.; Sharifzadeh, M. Application of response surface methodology for optimization of lead biosorption in an aqueous solution by *Aspergillus niger*. *J. Hazard. Mater.* **2008**, *154*, 694–702. [[CrossRef](#)]
28. Heidari, A.; Younesi, H.; Mehraban, Z. Removal of Ni(II), Cd(II), and Pb(II) from a ternary aqueous solution by amino functionalized mesoporous and nano mesoporous silica. *Chem. Eng. J.* **2009**, *153*, 70–79. [[CrossRef](#)]
29. Yin, J.; Deng, C.; Yu, Z.; Wang, X.; Xu, G. Effective removal of lead ions from aqueous solution using nano illite/smectite clay: Isotherm, kinetic, and thermodynamic modeling of adsorption. *Water* **2018**, *10*, 210. [[CrossRef](#)]
30. Haider, S.; Park, S.-Y. Preparation of the electrospun chitosan nanofibers and their applications to the adsorption of Cu(II) and Pb(II) ions from an aqueous solution. *J. Membr. Sci.* **2009**, *328*, 90–96. [[CrossRef](#)]
31. Zhang, C.; Li, X.; Pang, J. Synthesis and adsorption properties of magnetic resin microbeads with amine and mercaptan as chelating groups. *J. Appl. Polym. Sci.* **2001**, *82*, 1587–1592. [[CrossRef](#)]
32. Lagergren, S.; Sevensk, B. Zur theorie der sogenannten adsorption gelöster stoffe. *Vantens Kapsa Kedhandle* **1898**, *24*, 134–178.
33. Li, G.; Cai, W.; Zhao, R.; Hao, L. Electrosorptive removal of salt ions from water by membrane capacitive deionization (MCDI): Characterization, adsorption equilibrium, and kinetics. *Environ. Sci. Pollut. Res.* **2019**, *1*–10. [[CrossRef](#)] [[PubMed](#)]
34. Javadian, H.; Ahmadi, M.; Ghiasvand, M.; Kahrizi, S.; Katal, R. Removal of Cr(VI) by modified brown algae *Sargassum bevanom* from aqueous solution and industrial wastewater. *J. Taiwan Inst. Chem. Eng.* **2013**, *44*, 977–989. [[CrossRef](#)]
35. Katal, R.; Hasani, E.; Farnam, M.; Baei, M.S.; Ghayyem, M.A. Charcoal ash as an adsorbent for Ni(II) adsorption and its application for wastewater treatment. *J. Chem. Eng. Data* **2012**, *57*, 374–383. [[CrossRef](#)]
36. Azizian, S. Kinetic models of sorption: A theoretical analysis. *J. Colloid Interface Sci.* **2004**, *276*, 47–52. [[CrossRef](#)]
37. Chen, A.-H.; Liu, S.-C.; Chen, C.-Y.; Chen, C.-Y. Comparative adsorption of Cu(II), Zn(II), and Pb(II) ions in aqueous solution on the crosslinked chitosan with epichlorohydrin. *J. Hazard. Mater.* **2008**, *154*, 184–191. [[CrossRef](#)]
38. Debbaudt, A.; Ferreira, M.; Gschaider, M. Theoretical and experimental study of  $M^{2+}$  adsorption on biopolymers. III. Comparative kinetic pattern of Pb, Hg and Cd. *Carbohydr. Polym.* **2004**, *56*, 321–332. [[CrossRef](#)]
39. Genç, Ö.; Soysal, L.; Bayramoğlu, G.; Arica, M.; Bektaş, S. Procion Green H-4G immobilized poly (hydroxyethylmethacrylate/chitosan) composite membranes for heavy metal removal. *J. Hazard. Mater.* **2003**, *97*, 111–125. [[CrossRef](#)]
40. Sun, S.; Wang, L.; Wang, A. Adsorption properties of crosslinked carboxymethyl-chitosan resin with Pb(II) as template ions. *J. Hazard. Mater.* **2006**, *136*, 930–937. [[CrossRef](#)]
41. Moradi, O.; Aghaie, M.; Zare, K.; Monajjemi, M.; Aghaie, H. The study of adsorption characteristics  $Cu^{2+}$  and  $Pb^{2+}$  ions onto PHEMA and P (MMA-HEMA) surfaces from aqueous single solution. *J. Hazard. Mater.* **2009**, *170*, 673–679. [[CrossRef](#)] [[PubMed](#)]
42. Banerjee, M.; Basu, R.K.; Das, S.K. Cu(II) removal using green adsorbents: Kinetic modeling and plant scale-up design. *Environ. Sci. Pollut. Res.* **2018**, *6*, 11542–11557. [[CrossRef](#)] [[PubMed](#)]
43. Katal, R.; Baei, M.S.; Rahmati, H.T.; Esfandian, H. Kinetic, isotherm and thermodynamic study of nitrate adsorption from aqueous solution using modified rice husk. *J. Ind. Eng. Chem.* **2012**, *18*, 295–302. [[CrossRef](#)]



© 2019 by the authors. Licensee MDPI, Basel, Switzerland. This article is an open access article distributed under the terms and conditions of the Creative Commons Attribution (CC BY) license (<http://creativecommons.org/licenses/by/4.0/>).